PADOVA UNIVERSITY PRESS

Dolomites Research Notes on Approximation

Special issue dedicated to Annie Cuyt on the occasion of her 60th birthday, Volume 10 · 2017 · Pages 128–137

# Spectral filtering for the reduction of the Gibbs phenomenon for polynomial approximation methods on Lissajous curves with applications in MPI

Stefano De Marchi[a] · Wolfgang Erb[b] · Francesco Marchetti[a]

*Communicated by A. Weinmann*

**Abstract**

Polynomial interpolation and approximation methods on sampling points along Lissajous curves using Chebyshev series is an effective way for a fast image reconstruction in Magnetic Particle Imaging. Due to the nature of spectral methods, a Gibbs phenomenon occurs in the reconstructed image if the underlying function has discontinuities. A possible solution for this problem are spectral filtering methods acting on the coefficients of the approximating polynomial.
In this work, after a description of the Gibbs phenomenon and classical filtering techniques in one and several dimensions, we present an adaptive spectral filtering process for the resolution of this phenomenon and for an improved approximation of the underlying function or image. In this adaptive filtering technique, the spectral filter depends on the distance of a spatial point to the nearest discontinuity. We show the effectiveness of this filtering approach in theory, in numerical simulations as well as in the application in Magnetic Particle Imaging.

## 1 Introduction

Magnetic Particle Imaging (MPI) is an emerging medical imaging technology which attracted the interest of different research groups in the last years [14]. This imaging technology is based on the detection of a tracer consisting of superparamagnetic iron oxide nanoparticles through the superimposition of different magnetic fields.

When the magnetic tracer particles are excited by oscillating magnetic fields, electromagnetic induction generates a voltage signal in properly positioned receive coils. The magnetic fields are generated in such a way that the acquisition of the signal is performed following a field-free point along a suitable sampling trajectory.

One possible choice for such sampling trajectories are Lissajous curves [15]. For the reconstruction of the magnetic particle densities, these curves have a series of advantages, among others, particular sampling points on the curves can be used directly to obtain a polynomial reconstruction of the density [10, 13].

Particular Lissajous curves for polynomial interpolation and approximation were considered in the framework of the *Padua points* [6, 4, 3]. These points form a unisolvent set for polynomial interpolation of total degree in the square, they are explicitly known and the Lebesgue constant of their interpolation scheme is of minimal growth. For further information, references and software see the web page [23]. Due to their excellent properties, efforts have been made in order to understand more about these points for general Lissajous curves. Bivariate Lissajous node points which are provided with properties similar to the Padua points, were introduced and studied in [10, 11]. Three- and higher dimensional Lissajous curves have been recently studied in [1, 2, 9]. Wheras in [9] particular Lissajous are considered that allow multivariate polynomial interpolation, in [1, 2] a hyperinterpolation polynomial approximation for Lissajous curves with conjectured optimal parameters has been carried out. This method consists in using a discretized orthogonal projection of a function into a space of orthogonal polynomials of a fixed total degree.

The polynomial interpolants and hyperinterpolants can be expressed as multivariate Chebyshev series which, by a change of coordinates, can be expressed also as Fourier series. In applications, many objects are represented by discontinuous functions. In this case, it is well-known that the presence of discontinuities in the function gives rise to the so called *Gibbs phenomenon*. The Gibbs phenomenon causes distortions in the image reconstruction, providing oscillations near the leap points of the function which affect the whole image. This phenomenon is already widely treated in the literature, see for example [5, 18].

In this work, we study the Gibbs phenomenon and possible resolutions of this problem in the context of polynomial interpolation on Lissajous node points and in view of applications in MPI. To this end, we review the usage of classical Fourier spectral filtering [12], we introduce an adaptive spectral filtering process to diminish the Gibbs oscillations and we show its efficiency in theory, in numerical simulations as well as in some MPI examples. In particular, we proceed as follows: in the next section, we introduce the Lissajous node points which can be obtained from degenerated or non-degenerated Lissajous curves [11]. For instance, in

[a]Department of Mathematics "Tullio Levi-Civita", University of Padova, Italy
[b]Department of Mathematics, University of Hawai'i at Mānoa, USA

MPI applications we must choose non-degenerate curves as specified in [10]. Indeed, in this case the centre of the square $[-1,1]^2$ is a Lissajous node which is useful in order to calibrate the MPI scanner.
In Section 3, we give a presentation about multi-dimensional Fourier series and the Gibbs phenomenon. In Section 4, classical Fourier spectral filters are presented. First, we review the one-dimensional case and then we introduce corresponding filters in the general multi-dimensional setting such that fundamental properties as the reduction of the Gibbs phenomenon are preserved. In Section 5, we present a bivariate adaptive filtering process based on the univariate approach given in [20]. In Section 6, we first modify the adaptive parameter of the filter in order to resolve some distortions appearing in the results of the experiments, and make a conjecture about a new promising adaptive parameter. Then, we show that the usage of this new parameter improves the final result of the reconstruction in some MPI simulations.

## 2 Lissajous curves and its nodes in the square

Let $Q_2 = [-1,1]^2$ and let $\boldsymbol{n} = (n_1, n_2) \in \mathbb{N}^2$ such that $n_1, n_2$ are relatively prime. We consider the two-dimensional parametric Lissajous curve $\gamma_\epsilon^{\boldsymbol{n}} : I \to Q_2$ defined as

$$\gamma_\epsilon^{\boldsymbol{n}}(t) := \begin{pmatrix} \cos(n_2 t) \\ \cos(n_1 t - (\epsilon-1)\pi/(2n_2)) \end{pmatrix} \tag{1}$$

with $\epsilon \in \{1,2\}$. If $\epsilon = 1$ then $I = [0,\pi]$ and the curve is *degenerate*, if $\epsilon = 2$ then $I = [0,2\pi]$ and the curve is *non-degenerate*. In both cases, the Lissajous curve is $2\pi$-periodic. The degenerate curve $\gamma_1^{\boldsymbol{n}}(t)$ is however traversed twice as $t$ varies from 0 to $2\pi$. Although a more general definition can be given [11], the definition (1) is sufficient for the applications we consider.

*Observation* 1. The Lissajous curve generating one of the 4 families of the Padua points (see [3, 4]) can be written, up to a reflection with respect to one of the coordinate axis, in the form $\gamma_1^{(n,n+1)}$ or $\gamma_1^{(n+1,n)}$. One of the families of Morrow-Patterson points considered in [17] can be generated by the curve $\gamma_1^{(n+2,n+3)}$, as they consist in the self-intersection points of such a curve.

We are interested in the sets of points generated by Lissajous curves, in the sense given by the following definition.

*Definition* 1. Let $\gamma_\epsilon^{\boldsymbol{n}}$ be a Lissajous curve with $\epsilon \in \{1,2\}$ and let

$$t_k^{\epsilon \boldsymbol{n}} := \frac{\pi k}{\epsilon n_1 n_2}, \; k = 0, \ldots, 2\epsilon n_1 n_2 - 1. \tag{2}$$

The set

$$\mathrm{LS}_\epsilon^{\boldsymbol{n}} := \{\gamma_\epsilon^{\boldsymbol{n}}(t_k^{\epsilon \boldsymbol{n}}) : k = 0, \ldots, 2\epsilon n_1 n_2 - 1\} \tag{3}$$

is the set of Lissajous node points related to $\gamma_\epsilon^{\boldsymbol{n}}$.

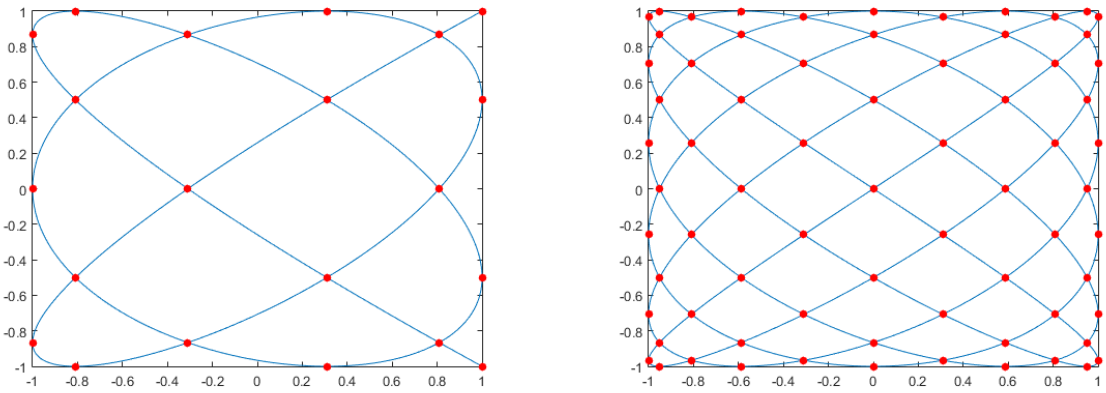

**(a)** The degenerate curve $\gamma_1^{(5,6)}$. **(b)** The non-degenerate curve $\gamma_2^{(5,6)}$.

**Figure 1:** Two examples of Lissajous curves and nodes.

We define also the following index set associated to Lissajous nodes

$$\Gamma^{\epsilon \boldsymbol{n}} := \left\{(i,j) \in \mathbb{N}_0^2 \; : \; \frac{i}{\epsilon n_1} + \frac{j}{\epsilon n_2} < 1\right\} \cup \{(0, \epsilon n_2)\} \tag{4}$$

and consider the polynomial space on $Q_2$:

$$\Pi^{\epsilon \boldsymbol{n}} := \mathrm{span}\{\hat{\phi}_{ij}(\boldsymbol{x}) \; : \; (i,j) \in \Gamma^{\epsilon \boldsymbol{n}}\}. \tag{5}$$

Here

$$\hat{\phi}_{ij}(\boldsymbol{x}) = \hat{T}_i(x_1)\hat{T}_j(x_2), \tag{6}$$

where $\hat{T}_0(x_1)=1$, $\hat{T}_i(x_1)=\sqrt{2}\cos(i\arccos(x_1))$ for $i\geq 1$ is the normalized $i$-th Chebyshev polynomial of the first kind.
As derived in [11], we can express the polynomial interpolant $\mathcal{L}^{\epsilon n}f$ in the space $\Pi^{\epsilon n}$ of a given function $f$ as

$$\mathcal{L}^{\epsilon n}f(\boldsymbol{x})=\sum_{(i,j)\in\Gamma^{\epsilon n}} c_{ij}(f)\hat{\phi}_{ij}(\boldsymbol{x}), \tag{7}$$

where the coefficients $c_{ij}(f)$ are uniquely given by the values of the function $f$ on the point set $\mathrm{LS}_\epsilon^n$. Using the change of variables $x=\cos(t)$, $y=\cos(s)$, and expanding the set $\Gamma^{\epsilon n}$ in

$$\Gamma_S^{\epsilon n}:=\Big\{(i,j)\in\mathbb{Z}^2\ :\ (|i|,|j|)\in\Gamma^{\epsilon n}\Big\}. \tag{8}$$

we can express the interpolant $\mathcal{L}^{\epsilon n}f$ as the Fourier series

$$\mathcal{L}^{\epsilon n}f(t,s)=\sum_{(i,j)\in\Gamma_S^{\epsilon n}}\tilde{c}_{ij}(f)\,e_i(t)e_j(s), \tag{9}$$

where $e_j(s)=e^{\mathrm{i}js}$.

## 3 Fourier series and the Gibbs phenomenon

Let $f:\mathbb{R}^\nu\to\mathbb{R}$ be a measurable real-valued function which is $2\pi$-periodic in all of its $\nu\in\mathbb{N}$ arguments. For $1\leq p\leq\infty$, $\boldsymbol{x}=(x_1,x_2,\ldots,x_\nu)$, we consider the function space

$$L^p_{2\pi}(\mathbb{R}^\nu)=\left\{f:\mathbb{R}^\nu\to\mathbb{R}\text{ measurable, }2\pi\text{-periodic and }(2\pi)^{-\nu}\int_{(-\pi,\pi)^\nu}|f(\boldsymbol{x})|^p\mathrm{d}\boldsymbol{x}<\infty\right\}, \tag{10}$$

where $\mathrm{d}\boldsymbol{x}$ is the $\nu$-dimensional Lebesgue measure, and the (semi)-norm

$$\|f\|_p:=\begin{cases}(2\pi)^{-\nu}\Big(\displaystyle\int_{(-\pi,\pi)^\nu}|f(\boldsymbol{x})|^p\mathrm{d}\boldsymbol{x}\Big)^{1/p} & \text{if } 1\leq p<\infty,\\ \displaystyle\sup_{\boldsymbol{x}\in\mathbb{R}^\nu}|f(\boldsymbol{x})| & \text{if } p=\infty.\end{cases} \tag{11}$$

For $f\in L^1_{2\pi}(\mathbb{R}^\nu)$, the multidimensional Fourier series of $f$ (in complex form) is defined as

$$Sf(\boldsymbol{x})=\sum_{\boldsymbol{n}\in\mathbb{Z}^\nu}c_{\boldsymbol{n}}(f)e_{\boldsymbol{n}}(\boldsymbol{x}),\quad \boldsymbol{x}\in\mathbb{R}^\nu, \tag{12}$$

$$c_{\boldsymbol{n}}(f)=(2\pi)^{-\nu}\int_{(-\pi,\pi)^\nu}f(\boldsymbol{x})\overline{e_{\boldsymbol{n}}(\boldsymbol{x})}\mathrm{d}\boldsymbol{x}. \tag{13}$$

where $e_{\boldsymbol{n}}(\boldsymbol{x}):=\prod_{j=1}^\nu e_{n_j}(x_j)$ is the tensor product Fourier basis.
Moreover, for $N\in\mathbb{N}$, we introduce the partial Fourier sum

$$S_Nf(\boldsymbol{x})=\sum_{\substack{\boldsymbol{k}\in\mathbb{Z}^\nu\\ \|\boldsymbol{k}\|_\infty\leq N}}c_{\boldsymbol{k}}(f)e_{\boldsymbol{k}}(\boldsymbol{x}),\ \boldsymbol{x}\in\mathbb{R}^\nu, \tag{14}$$

where $\|\boldsymbol{k}\|_\infty=\|(k_1,k_2,\ldots,k_\nu)\|_\infty=\sup\{|k_1|,|k_2|,\ldots,|k_\nu|\}$.
The theory of Fourier series can be applied also to approximate integrable functions which are defined on a more general bounded domains. In order to do this and to preserve a possible continuity of the function, symmetrization and periodic extension techniques can be applied. In applications, we often deal with functions that are discontinuous and piecewise regular, in the sense given by the following definition.

*Definition* 2. Let $\Omega\subset\mathbb{R}^\nu$ be bounded, open and Lipschitz, and $f:\Omega\to\mathbb{R}$. We say that $f$ is piecewise regular, if there exists a Lipschitz partition $(\Omega_i)_{i=1,\ldots,n}$ of $\Omega$, where $\Omega_i$ is an open set with Lipschitz boundary for every $i=1,\ldots,n$, and regular functions $f_i:\Omega_i\to\mathbb{R}$ such that $f$ coincides with $f_i$ on $\Omega_i$ for all $i=1,\ldots,n$.

From now on we consider discontinuous and piecewise regular functions. The exact regularity class of the functions $f_i$ will be relevant only later on for particular error estimates.
It is well-known that if we try to approximate such functions through a Fourier series then the *Gibbs phenomenon* arises. This phenomenon is caused by the slow decay (first order) of the Fourier coefficients $|c_{\boldsymbol{k}}(f)|$ as $N$ in the series (14) becomes larger. Further, it affects the reconstruction of a function as distortions and oscillations are generated on the whole domain and, in particular, close to the discontinuities. A more detailed discussion of this phenomenon in one and several dimensions is provided in [16].
In the following lines, we take as example the function $g:[-1,1]^2\to\mathbb{R}$ defined as

$$g(x,y)=\begin{cases}1 & x^2+y^2\leq(0.6)^2,\\ 0 & \text{otherwise.}\end{cases} \tag{15}$$

The function $g$ and the appearance of the Gibbs phenomenon in its polynomial approximation are displayed in Figure 2.

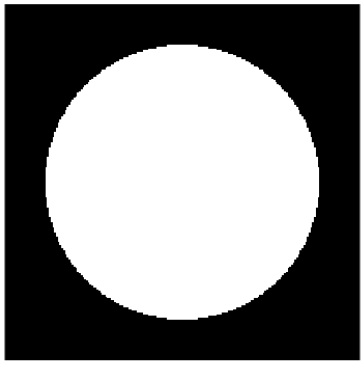

**(a)** The original function $g$ given in (15).

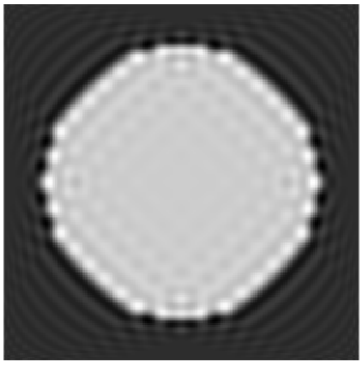

**(b)** Polynomial approximation $\mathcal{L}^{64,66}g$ interpolating $g$ along the curve $\gamma_2^{(32,33)}$.

**Figure 2:** Example of the Gibbs phenomenon for polynomial interpolation of the indicator function for a disk.

## 4 Fourier spectral filters

A possible solution for the problem presented in the previous section is to accelerate the decay rate of the coefficients in the sum (14) by using appropriate spectral filter functions. It is well-known that the Gibbs phenomenon does not disappear just by cutting down the high coefficients, so a step function would be useless as a filter. To this aim, we introduce the following definition of a *spectral filter of order p* (cf. [12, Def 3.1, p.650]).

*Definition* 3. An even function $\sigma : \mathbb{R} \to \mathbb{R}$ is called a spectral filter of order $p$ if:

1. $\sigma \in C^{p-1}$.
2. $\sigma(0) = 1$, $\sigma^{(l)}(0) = 0$ for $1 \le l \le p-1$.
3. $\sigma(\eta) = 0$ for $|\eta| \ge 1$.

These conditions provide smooth and bell-shaped filter functions that have compact support. The compact support of $\sigma$ ensures that the corresponding filtered Fourier series (21) is a finite sum of trigonometric basis functions. Condition 2. is a regularity condition and guarantees almost vanishing moments of order $p$ of the mollifier function (24) in the space domain, cf. [20, Theorem 2.2].

Some examples of filters for $|\eta| \le 1$ are (cf. [12, p. 654]) :

- The FejÃ©r filter (first order)
$$\sigma(\eta) = 1 - |\eta|. \tag{16}$$
- The Lanczos or sinc filter (first order)
$$\sigma(\eta) = \frac{\sin(\pi\eta)}{\pi\eta}. \tag{17}$$
- The *raised cosine* filter (second order)
$$\sigma(\eta) = \frac{1}{2}(1 + \cos(\pi\eta)). \tag{18}$$
- The exponential filter of order $p$ ($p$ even)
$$\sigma(\eta) = e^{-\alpha|\eta|^p}. \tag{19}$$
In this case, since $\sigma(1) = e^{-\alpha}$, the exponential filter does not respect the formal definition of filter. In applications, we set the value of $\alpha$ such that $e^{-\alpha}$ is in the range of the computer's roundoff error.

It is well-known (see for example [12]) that such a filtering process provides a reduction of the uniform error $\|f - S_N^\sigma f\|_\infty$ away from the discontinuities.

Now, let $\sigma$ be a spectral filter according to Definition 3. For a fixed $N \in \mathbb{N}$, we can consider the sequence $(\sigma_k)_{k\in\mathbb{Z}}$ given by

$$\sigma_k = \sigma\left(\frac{k}{N}\right), \quad k \in \mathbb{Z}, \tag{20}$$

and introduce the filtered Fourier series

$$S_N^\sigma f(x) = \sum_{k\in\mathbb{Z}} \sigma_k c_k(f) e_k(x). \tag{21}$$

We construct a tensor product pattern of $\nu$ one-dimensional filters

$$\boldsymbol{\sigma}_{\boldsymbol{k}} = \sigma_{k_1}\sigma_{k_2}\cdots\sigma_{k_\nu} = \sigma\left(\frac{k_1}{N}\right)\sigma\left(\frac{k_2}{N}\right)\cdots\sigma\left(\frac{k_\nu}{N}\right),\ -N \le k_1, k_2, \ldots, k_\nu \le N \tag{22}$$

so that we can generalize the series (21) to the multi-dimensional setting by

$$S_N^\sigma f(\boldsymbol{x}) = \sum_{\boldsymbol{k}\in\mathbb{Z}^\nu} \boldsymbol{\sigma}_{\boldsymbol{k}} c_{\boldsymbol{k}}(f) e_{\boldsymbol{k}}(\boldsymbol{x}). \tag{23}$$

Using the variable $\boldsymbol{\eta} = (\eta_1, \eta_2, \ldots, \eta_\nu)$, the underlying function $\boldsymbol{\sigma}(\boldsymbol{\eta}) = \sigma(\eta_1)\sigma(\eta_2)\cdots\sigma(\eta_\nu)$ is well defined and has similar properties of the univariate function. Indeed, it is easy to observe that if $\sigma$ is a one-dimensional filter of order $p$ and $\boldsymbol{\alpha} = (\alpha_1, \alpha_2, \ldots, \alpha_\nu) \in \mathbb{Z}^\nu_{\ge 0}$, $\boldsymbol{\alpha} \neq \boldsymbol{0}$, then:

1. $\boldsymbol{\sigma} \in C^{p-1}$.
2. $\boldsymbol{\sigma}(\boldsymbol{0}) = 1$, $(D^{\boldsymbol{\alpha}}\boldsymbol{\sigma})(\boldsymbol{0}) = 0$ for $1 \le |\boldsymbol{\alpha}| \le p-1$, where $D^{\boldsymbol{\alpha}}$ is the usual multi-dimensional derivative of $\boldsymbol{\sigma}$ with respect to the multi-index $\boldsymbol{\alpha}$.
3. $\boldsymbol{\sigma}(\boldsymbol{\eta}) = 0$ for $\|\boldsymbol{\eta}\|_\infty \ge 1$.

In particular, it follows that the function $\boldsymbol{\sigma}$ acts on high multi-variate frequences in a similar way as $\sigma$ does in the univariate case.

## 5 Adaptive spectral filtering

Spectral filters as introduced in the previous section act on the Fourier coefficients and do not consider the physical position of the discontinuities. It is known that the operation of such spectral filters is equivalent to mollification in the physical space. Indeed, defining the mollifier

$$\Phi^\sigma(y) := \frac{1}{2\pi}\sum_{k\in\mathbb{Z}} \sigma_k e_k(y) \tag{24}$$

we can write

$$S_N^\sigma f(x) \equiv f * \Phi^\sigma(x) = \int_{-\pi}^{\pi} \Phi^\sigma(y) f(x-y)\mathrm{d}y. \tag{25}$$

This global mollification does not differentiate between different regions in space and yields blurred images (see for instance Figure 3 (a)) if the global filter is too strong, or has no impact on the Gibbs phenomenon if the filter is too weak. It is therefore reasonable to consider filters that apply a strong filtering on the function $f$ only in the region in which the discontinuities are located. To this end, we consider the following adaptive filter function introduced in [20]

$$\sigma^p(\eta) = \begin{cases} \exp\left(\dfrac{|\eta|^p}{\eta^2-1}\right) & |\eta| < 1\,, \\ 0 & |\eta| \ge 1\,, \end{cases} \tag{26}$$

where $p : \mathbb{R} \to \mathbb{R}_+$ is a function depending on the position $x$. In our discussion, the parameter function $p = p(x)$ is the key for the adaptivity. Since $p > 0$ is not necessarily a natural number, we use the notation

$$\|f\|_{C^p} = \max_{k\le p} \|f^{(k)}\|_\infty, \quad k \in \mathbb{N}, \tag{27}$$

$$p! = \Gamma(p+1). \tag{28}$$

We restrict our discussion to the two-dimensional case. However, all given considerations are true also in a higher-dimensional setting. For $\boldsymbol{y} = (y_1, y_2) \in \mathbb{R}^2$ and $\boldsymbol{p} = (p_1, p_2)$, we set

$$\Phi^{\boldsymbol{\sigma}^{\boldsymbol{p}}}(\boldsymbol{y}) := \frac{1}{4\pi^2}\sum_{\boldsymbol{k}\in\mathbb{Z}^2} \boldsymbol{\sigma}^{\boldsymbol{p}}_{\boldsymbol{k}} e_{\boldsymbol{k}}(\boldsymbol{y}), \tag{29}$$

where

$$\boldsymbol{\sigma}^{\boldsymbol{p}}_{\boldsymbol{k}} = \sigma^{p_1}_{k_1}\sigma^{p_2}_{k_2}, \tag{30}$$

and the filter functions $\sigma^{p_i}_{k_i}$, $i \in \{1,2\}$, are given as in (26).

Let $\boldsymbol{\xi} = (\xi_1, \xi_2)$ be the closest point of discontinuity with respect to a point $\boldsymbol{x} = (x_1, x_2)$ in the euclidean norm. For $i = 1, 2$, we set $\delta_i(\boldsymbol{x}) = |x_i - \xi_i|$. Note that the two distance functions $\delta_1$ and $\delta_2$ depend on both variables $x_1$ and $x_2$.

*Lemma* 1. Let $\sigma^p$ be as defined in (26). Then there exist constants $M_\sigma, \eta_\sigma > 0$ independent from $p$ such that

$$\|\sigma^p\|_{C^p} \le M_\sigma (p!)^2 \eta_\sigma^{-p}. \tag{31}$$

*Proof.* See [20] Lemma 2.1. □

Using Lemma (1), we obtain the following error estimate for adaptive filtering.

*Theorem* 2. Let $f : \Omega \subset \mathbb{R}^2 \to \mathbb{R}$ be a piecewise analytic function on some open bounded Lipschitz domain $\Omega$. Then, setting

$$\boldsymbol{p} = (p_1(\boldsymbol{x}), p_2(\boldsymbol{x})) = ((N\eta_1^*\delta_1(\boldsymbol{x}))^{1/2}, (N\eta_2^*\delta_2(\boldsymbol{x}))^{1/2}), \tag{32}$$

with suitable choosen parameters $\eta_1^*, \eta_2^*$, the error $|f - S_N^{\sigma^p} f|$ decays with an asymptotic exponential rate away from the points of discontinuity of $f$. Here, the adaptive approximant $S_N^{\sigma^p} f$ is given by $S_N^{\sigma^p} f = f * \Phi^{\sigma^p}$ with the mollifier $\Phi^{\sigma^p}$ defined in (29) and the parameters $p_1, p_2$ given in (32).

*Proof.* The proof combines a tensor product approach with univariate arguments given in [20]. In order to reduce it to the result [20, Theorem 2.1] of the univariate case, particular care has to be given to the correct implementation of the adaptivity strategy (32) and a proper splitting of the involved double sums. The details are elaborated in [16] p.28–33. □

**Remarks**

- In this section we required the analyticity of $f$ away from its discontinuities. If $f$ is not analytic, the exponential convergence of the approximation error is in general lost and, depending on the regularity of the function, a subexponential or polynomial decay rate is obtained.
- The tensor product structure allows us to extend this result also to a general $\nu$-dimensional setting, the adaptive parameter then becomes
$$\boldsymbol{p} = \left((N\eta_1^*\delta_1(\boldsymbol{x}))^{1/2}, (N\eta_2^*\delta_2(\boldsymbol{x}))^{1/2}, \ldots, (N\eta_\nu^*\delta_\nu(\boldsymbol{x}))\right)^{1/2}.$$
- Note that the functions $\delta_i(\boldsymbol{x})$ are not necessarily continuous at all points $\boldsymbol{x}$, so that also $S_N^{\sigma^p} f$ in Theorem 2 is also not necessarily a continuous function. This results in striped distortions in the filtered images as can be seen in Figure 3 (b). To define $\delta_i(\boldsymbol{x})$ in case there is no unique closest discontinuity, one can take the average distance over all possible closest points.

## 6 Numerics

In this section we first modify the adaptive parameter of the filter with the aim to resolve some distortions appearing in the results of the experiments, making a conjecture about a new *adaptive parameter*. Then, we show that the usage of this new parameter improves the final result of the reconstruction also in MPI simulations.

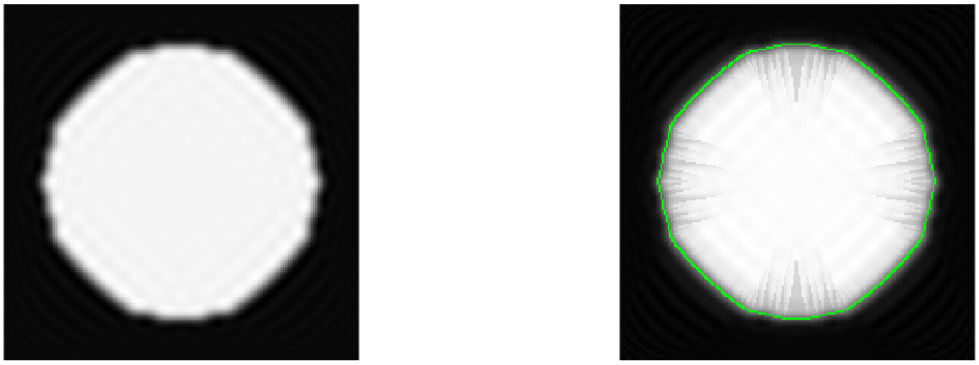

**(a)** Spectrally filtered polynomial $\mathcal{L}^{(64,66)}g$ using the raised cosine filter (18).

**(b)** Spectrally filtered polynomial $\mathcal{L}^{(64,66)}g$ using the distorted adaptive spectral filtering.

**Figure 3:** Approximation of the function $g$ with filtered polynomial interpolants. The adaptive filter in b) is based on the strategy (33) with the parameters $(n_1, n_2) = (32, 33)$ and $\eta = 0.23$. The edges (marked in green) were determined using the Canny edge detector [7], see Section 6.2.

### 6.1 Modification of the adaptive parameter

We consider again the bivariate setting. In order to use the adaptive parameter $\boldsymbol{p}$ in the spectral filtering process for the interpolating polynomial at the Lissajous nodes $\mathrm{LS}^{\epsilon n}$, we slightly alter the parameter $\boldsymbol{p}$ in (32). We set

$$\boldsymbol{p} = \left((\eta n_1\delta_1(\boldsymbol{x}))^{1/2}, (\eta n_2\delta_2(\boldsymbol{x}))^{1/2}\right), \tag{33}$$

where $n_1, n_2$ are the underlying frequency parameters of the Lissajous curve and $\eta = \eta_1^* = \eta_2^*$ is an appropriate constant. We observed in [16] that (see also Figure 3), using the adaptive parameter (33) similar to the one suggested in Theorem 2, the filtered image gets affected by striped distortions which are generated at the discontinuities of the functions $\delta_1(\boldsymbol{x})$ and $\delta_2(\boldsymbol{x})$.

In order to improve the final result and to avoid the appearance of these stripes, we can modify the definition of the adaptive parameters trying to improve our result. We point out that the following part of this section is conjectured from experiments and observations and is not supported by the theory as before.

Instead of the two parameters $p_1, p_2$ considered so far, we can consider a unique parameter $p$ which depends on the Euclidean distance

$$d(\boldsymbol{x}) = \|\boldsymbol{x} - \boldsymbol{\xi}\|_2 = \sqrt{\delta_1(\boldsymbol{x})^2 + \delta_2(\boldsymbol{x})^2}. \tag{34}$$

Note that in comparison to $\delta_1(\boldsymbol{x})$, $\delta_2(\boldsymbol{x})$ the function $d(\boldsymbol{x})$ is continuous. Letting $N = \sqrt{n_1^2 + n_2^2}$ and modifying the initial parameters as

$$p_1 = (\eta N \delta_1)^{1/2},\ p_2 = (\eta N \delta_2)^{1/2}, \tag{35}$$

we propose to take $p$ as follows

$$p = \sqrt{p_1^4 + p_2^4} = \eta N d(\boldsymbol{x}). \tag{36}$$

so that we can consider the adaptive parameter $\boldsymbol{p} = (p, p)$.
In the filtering process, we have to deal with two different situations. Using a strong filter, we get a robust reduction of the Gibbs phenomenon on the whole image, but we also cause a large smoothing effect close to the edges of the object represented by the function. On the other hand, using a weak filter we almost preserve the function near the discontinuities, but we can not greatly reduce the Gibbs phenomenon. Our aim is to find a trade-off between these two aspects.
Noticing that the parameter $p$ depends linearly on $d(\boldsymbol{x})$, we conjecture the following:

*Conjecture* 3. Let $\Phi : [0, +\infty) \to [0, +\infty)$ be a function such that:

- $\Phi(0) = 0$,
- $\Phi$ is a regular and increasing function in $[0, +\infty)$,
- $\Phi$ has a saturation property, that is there exists $\epsilon > 0$ such that

$$\Phi(x) \geq x \tag{37}$$

for $x \in [0, \epsilon]$.

Then, there exists a function $\Phi$ with these three properties, possibly depending on the function $f$, such that using the adaptive parameter

$$p = \eta N \Phi(d(\boldsymbol{x})) \tag{38}$$

the final result of the filtering process can be improved in terms of resolution of the Gibbs phenomenon and the accuracy of the approximation of the image.

A possible family of functions which have the described three properties and which we consider for our experiments is

$$\Phi_\beta(x) = x^\beta, \tag{39}$$

with $0 < \beta < 1$. For this family, we can define the new parameter

$$p_\beta = \eta N (d(\boldsymbol{x}))^\beta. \tag{40}$$

**Remark**
The new parameter $p_\beta$ is more sensitive and has a larger variation in small distances with respect to the linear one given in (36). On the other hand, $p_\beta$ has a saturation effect as the distance increases. Since we do not have theoretical guidelines, the tuning of the parameter $\beta$ is performed through an heuristic search. In our setting with a discretized grid of 201 points in the interval $[-1, 1]$, a suitable choice for the applications we have investigated so far is $\beta = 1/4$.

**Figure 4:** Spectrally filtered polynomial $\mathcal{L}^{(64,66)}g$ using the adaptive strategy (40) with $\beta = 1/4$ and $\eta = 0.0224$.

### 6.2 MPI applications

In the MPI reconstruction scheme described in [13], the density of the magnetic particles is derived by a measurement based approach, i.e. the MPI imaging operator is measured as a system matrix in a calibration procedure. To lower the costs, these measurements were reduced to the node points $LS^{\epsilon n}$ of a Lissajous curve, the sampling trajectories of MPI mentioned at the beginning of the manuscript. Once the reconstruction is performed on these sampling points by solving a linear system of equations (including the measured system matrix), the whole reconstruction of the particle density can be obtained by polynomial interpolation on the Lissajous node points. To obtain a filtered polynomial reconstruction, we proceed as follows.

1. Take the reconstructed particle density on the node points $LS^{\epsilon n}$ of the Lissajous curve as described in [13].
2. Obtain a first reconstruction by interpolating the function values on the Lissajous nodes $LS^{\epsilon n}$ using the polynomial interpolation described in Section 2, see also [10, 11].
3. Apply the first spectral filtering process as described in Section 4.
4. Use an edge-detector (in our case the Canny edge detector [7]) on the filtered reconstruction in order to find the edges and the distances required for the adaptivity.
5. Apply the final adaptive filtering procedure on the first reconstruction.

**Remarks**

- The Canny edge detector turned out to be a good choice for our purpose. A comparison between various edge detection algortihms is given in [8], where it is also mentioned that "*Canny proves the better detector for outer and inner lines of objects forming edges and has better immunity to noise than Sobel, Prewitt and Roberts detector*".
- To get for each point $\boldsymbol{x}$ its closest discontinuity point with respect to the Euclidan distance, we used the Matlab function $ipdm.m$ (Inter-Point Distance Matrix) by John D'Errico. The function is downloadable at the Matlab File Exchange of MathWorks.

In order to prove the effectiveness of our results, we used the SSIM (Structural SIMilarity index) parameter, which is a standard method for measuring the similarity between two images. The images we considered are two $201 \times 201$ matrices representing two phantoms: one consisting of a circle and the other consisting of two bars (see Fig. 5).

**Figure 5:** The original phantoms.

The experiments (in Matlab) were done by considering, as a domain containing our phantoms, the square $[-1,1]^2$ discretized as a grid of $201 \times 201$ points (which is the evaluation matrix). In order to include polynomial interpolation on Lissajous nodes, we modified and extended some functions of the $Chebfun$ 5.3.0 package [22]. The details are elaborated in the master thesis [16].

All reconstructions in $[-1,1]^2$ have been done using the node points $LS^{(66,64)}$ of a non-degenerate Lissajous curve of degree $(33,32)$ providing the parametric curve $\gamma_2^{(33,32)}$.

**Figure 6:** First reconstruction obtained by interpolating along the Lissajous curve.
SSIM= 0.665, SSIM= 0.616.

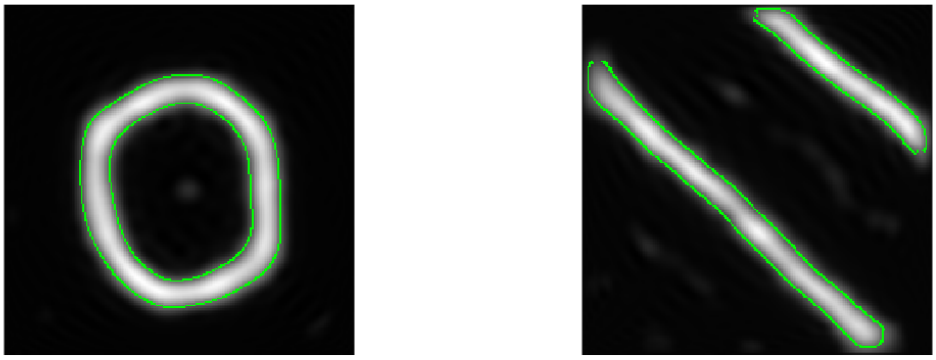

**Figure 7:** Final reconstruction using the adaptive filtering method described in Section 6.2 using a raised cosine filter for the first filtering and the parameters $\beta = 1/4, \eta = 0.0224$ for the final adaptive filtering. The edges detected by the Canny edge detector are marked in green. SSIM= 0.701, SSIM= 0.649.

In MPI, there exist various other ways than spectral methods to deal with the reconstrucion of images in the presence of edges and noise. A very efficient approach based on variational methods has been treated in [19].

## 7 Conclusions

Sampling along Lissajous curves followed by polynomial interpolation is an effective way to approximate functions without using a very large number of sampling points and it is a suitable procedure for MPI applications. However, in the reconstruction of discontinuous functions it is inevitable to face the Gibbs phenomenon.
Classic Fourier spectral filtering methods are efficient in diminishing the distortions given by the Gibbs phenomenon, but they also provide a general smoothing in the image and they cause a loss of definition. In our algorithm presented in this work, these classic spectral methods have been shown to be useful in order to improve the quality of the images prior to the application of edge-detectors and adaptive filtering methods.
Using the adaptive parameter suggested by the theory, the image reconstruction is affected by some distortions caused by the introduction of separated one-dimensional distances in a tensor product setting.
In order to improve the final result, we conjectured a different parameter depending on the euclidean distance between points and related closest discontinuities. After that, we presented a new idea using a non-linear dependence on the distance in the parameter. This brought an improvement in the general quality of the final reconstructed image.

As a future goal, we hope to improve these results in order to obtain more accuracy in the theory as well as an improved reconstruction quality in the application.

**Acknowledgement**
This work has been partially supported by the BIRD163015 and DOR funds of the University of Padova. This research has been accomplished within the RITA "Research ITalian network on Approximation".

## References


[1] Bos M., De Marchi S. and Vianello M. Trivariate polynomial approximation on Lissajous curves. *IMA J. Num. Anal.* 37(1) (2017), 519–541.

[2] Bos M., De Marchi S. and Vianello M. Polynomial approximation on Lissajous curves in the $d$-cube. *Appl. Numer. Math.* 116 (2017), 47–56.

[3] Bos L., Caliari M., De Marchi S., Vianello M. and Xu Y. Bivariate Lagrange interpolation at the Padua points: the generating curve approach. *J. Approx. Theory* 143 (2006), 15–25.

[4] Bos L., De Marchi S., Vianello M. and Xu Y. Bivariate Lagrange interpolation at the Padua points: the ideal theory approach. *Numer. Math.* 108(1) (2007), 43–57.

[5] Brezinski C. Extrapolation algorithms for filtering series of functions, and treating the Gibbs Phenomenon. *Numer. Algorithms* 36(4) (2004), 309–329.

[6] Caliari M., De Marchi S. and Vianello M. Bivariate polynomial interpolation on the square at new nodal sets. *Appl. Math. Comput.* 165(2) (2005), 261–274

[7] Canny J. A Computational Approach To Edge Detection. *IEEE Trans. Pattern Analysis and Machine Intelligence* 8(6) (1986), 679–698.

[8] Das S. Comparison of Various Edge Detection Technique. *International Journal of Signal Processing, Image Processing and Pattern Recognition* 9(2) (2016), 143–158.

[9] Dencker P., and Erb W. Multivariate polynomial interpolation on Lissajous-Chebyshev nodes. *arXiv:1511.04564 [math.NA]* (2015).

[10] Erb W., Kaethner C., Ahlborg M. and Buzug T.M. Bivariate Lagrange interpolation at the node points of non-degenerate Lissajous nodes. *Numer. Math.* 133(4) (2016), 685–705.

[11] Erb W., Kaethner C., Dencker P., and Ahlborg M. A survey on bivariate Lagrange interpolation on Lissajous nodes. *Dolomites Res. Notes Approx.* 8 (2015), 23–36.

[12] Gottlieb D. and Shu C. On the Gibbs phenomenon and its resolution. *SIAM Rev*, 39(4) (1997), 644–668.

[13] Kaethner C., Erb W., Ahlborg M., Szwargulski P., Knopp T. and Buzug T. M. Non-Equispaced System Matrix Acquisition for Magnetic Particle Imaging based on Lissajous Node Points. *IEEE Transactions on Medical Imaging*, 35(11) (2016), 2476–2485.

[14] Knopp T. and Buzug T. M. Magnetic Particle Imaging. *Springer* (2012).

[15] Knopp T., Biederer S., Sattel T., Weizenecker J., Gleich B., Borgert J. and Buzug T. M. Trajectory analysis for magnetic particle imaging. *Phys. Med. Biol.* 54(2) (2009), 385–397.

[16] Marchetti F. Spectral filtering for the resolution of the Gibbs phenomenon in MPI applications by Lissajous sampling. *Master thesis, University of Padova* (2016). http://tesi.cab.unipd.it/54084/

[17] Morrow C.R and Patterson T.N.L. Construction of Algebraic Cubature Rules Using Polynomial Ideal Theory. *SIAM J. Numer. Anal.* 15(5) (1978), 953–976.

[18] Navarra A., Stern W.F. and Miyakoda K. Reduction of the Gibbs oscillations in spectral model simulations. *Journal of Climate* 7(8) (1994), 1169–1183.

[19] Storath M., Brandt C., Hofmann M., Knopp T., Salamon J., Weber A. and Weinmann A. Edge Preserving and Noise Reducing Reconstruction for Magnetic Particle Imaging. *IEEE TMI* 36(1) (2017), 74–85.

[20] Tadmor E. and Tanner J. Adaptive filters for piecewise smooth spectral data. *IMA J. Num. Anal.* 25(4) (2005), 635–647.

[21] Wang Z., Bovik A.C., Sheikh H.R. and Simoncelli E.P. Image Quality Assessment: From Error Visibility to Structural Similarity. *IEEE Trans. Med. Imag.* 13(4) (2004), 600–612.

[22] Chebfun official website: http://www.chebfun.org

[23] Web page www.math.unipd.it/~marcov/CAApadua.html of the CAA group of the University of Padova and Verona